International Journal for Numerical Methods in Fluids
Int. J. Numer. Meth. Fluids **26**: 199–215 (1998)

VALIDATION OF TURBULENCE MODELS IN A SIMULATED AIR-CONDITIONING UNIT

Z.G. XU[a], D.H.T. GOTHAM[b,*], M.W. COLLINS[b], J.E.R. CONEY[c], C.G.W. SHEPPARD[c] AND S. MERDJANI[c]

[a] *Process Engineering Division, Silsoe Research Institute, Silsoe, Bedfordshire MK45 4HS, UK*
[b] *Thermo-Fluids Engineering Research Centre, City University, Northampton Square, London EC1V OHB, UK*
[c] *Department of Mechanical Engineering, University of Leeds, Leeds, UK*

SUMMARY

Details are given of a study to obtain experimental data in an idealized environment for the purpose of evaluating the corresponding computational predictions and which supplement parallel measurements made in actual packaged air-conditioning units. The system consisted of a purpose-built low-speed wind tunnel with a working section constructed to reproduce particular features of the real units. In the experiment, both the mean velocity profiles and turbulence properties of the flow are obtained from triple-hot-wire anemometry measurements. A numerical model, based on finite volume methodology, was used to obtain the solution of the Reynolds-averaged Navier–Stokes equations for incompressible isothermal flow. The Reynolds stress terms in the equations are calculated using the standard k–ϵ model and second-moment closure (Reynolds stress) models. The accuracy of the two models was evaluated against the experimental measurements made 10 mm downstream of a baffle. The results show that the standard k–ϵ model gave the better agreement except in regions of strong recirculation. © 1998 John Wiley & Sons, Ltd.

KEY WORDS: air-conditioning unit; k–ϵ model; Reynolds stress model

1. INTRODUCTION

Computational fluid dynamics (CFD) and heat transfer have matured to the stage where state-of-the-art commercial codes can address real engineering problems. These include three-dimensional, turbulent flow studies involving two phases with interphase heat and mass transfer. However, the advances in finite volume numerical capability which permit this, such as full three-dimensionality, generalized co-ordinate systems and multi-blocking, continue to require convincing validation procedures to demonstrate their quantitative engineering potential. This can most profitably be accomplished in carefully thought-out projects that permit direct comparison between the computational results and experimental measurements. It is not often that circumstances arise where it is possible to judge not only the accuracy of the primary variables but also the turbulence intensities which reflect the particular turbulence model selected for the numerical solution. One such case is the recent DTI–EPSRC LINK pro-

* Correspondence to: Thermo-Fluids Engineering Research Centre, City University, Northampton Square, London EC1V OHB, UK.

Contract grant sponsor: EPSRC/DTI (United Kingdom)

CCC 0271–2091/98/020199–17$17.50

Received November 1995
Revised March 1997

gramme involving Airedale International Air Conditioning Ltd., Leeds, the Department of Mechanical Engineering, the University of Leeds, the Thermo-Fluids Research Centre, City University, London and the Heat Transfer and Fluid Flow Service, National Engineering Laboratory, Glasgow. In this project the air flow pattern and heat transfer characteristics of a wide variety of packaged air-conditioning units were studied, both experimentally, using sophisticated instrumentation such as hot-wire anemometry, and numerically, employing two commercial CFD codes. The investigation was carried out in stages, starting with a unit in which only one component, the heat exchanger, was installed and progressively increasing the complexity of the unit. Parallel numerical and experimental data were obtained at each stage for comparison purposes.

In order to obtain experimental data in a situation that permitted the highest level of control over the test conditions, further investigations were undertaken in a wind tunnel in the Department of Mechanical Engineering, University of Leeds. Here the working section was used to model the configuration of one of the Airedale International packaged systems, the EHA5 unit, in which the air flows axially through components positioned in a rectangular duct. In the tests carried out on the packaged unit, it was found that one particular feature of the geometry of the system, the asymmetrical position of the coil within the outer casing with its supporting frame, caused areas of flow recirculation downstream of the frame [1]. In order to obtain additional experimental data in idealized flow conditions to augment the CFD validation, this particular configuration was reproduced in the working section of the wind tunnel by employing a system of offset baffles. A comparison between the velocity fields predicted numerically and measured experimentally has been presented elsewhere [1]. This paper is concerned with the second stage of validation, that of turbulence intensities and the choice of the turbulence model for the numerical computation.

2. EXPERIMENTAL INVESTIGATION

Shown in Figure 1 is the closed-circuit wind tunnel used for the experimental investigation; it is fully described by Coney *et al.* [2]. The air flow is provided by three axial fans in series, each of which may be controlled separately. The air velocity through the tunnel is dependent on the number of fans in use, with fine control being provided by a butterfly valve upstream of the fans. Downstream of the fans is a settling chamber, after which the air flows through a conditioning section, which permits the maintenance of dry-bulb temperature and relative humidity, as required; this comprises a dehumidification coil, a cooling coil, 3 kW electrical heater and a Vapac steam humidifier. After conditioning, the air flows through a convergence, followed by two right-angled bends, prior to entering the test section, which is connected to the main ducting by two flexible connections to minimize the transmission of fan vibration. Approaching the test section, the air dry-bulb temperature is measured by a thermocouple, which is checked against a standard mercury-in-glass thermometer. The air velocity is measured using a Prandtl pitot-static probe in conjunction with a micromanometer. A Vaisala HM132 electronic hygrometer is used to record the dry-bulb temperature and relative humidity with an accuracy of 0.3°C and 2%–3% respectively. It is placed at the centre of the duct, 1 m upstream of the test section, to minimize the effect on the air flow. The tunnel has a rectangular cross-section throughout and is constructed using 6 mm thick PVC sheeting. The low thermal conductivity of the material prevented heat loss from the tunnel, although there was external insulation in the form of polystyrene sheeting.

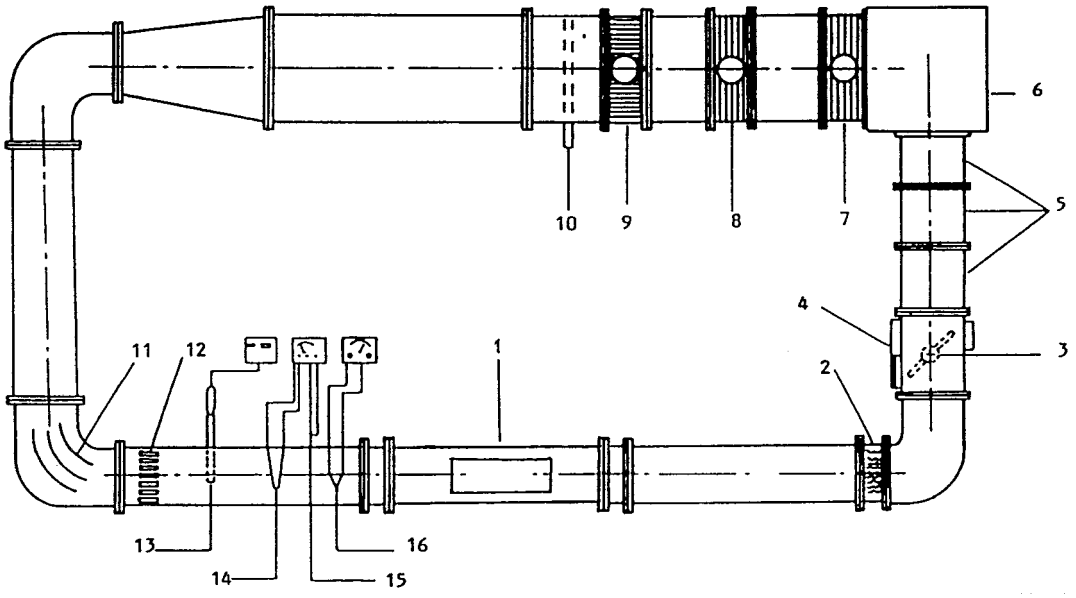

Figure 1. Diagram of Leeds University experimental wind tunnel: 1, test section; 2, water eliminator; 3, butterfly valve; 4, fresh air supply; 5, axial fans; 6, settling chamber; 7, dehumidifying coil; 8, cooling coil; 9, electric heater; 10, steam injectors; 11, guide vanes; 12, flow straightener; 13, electronic hygrometer; 14, multi-hole pitot-static probe; 15, Prandtl pitot-static probe; 16, wet and dry thermocouples

The test section, shown diagrammatically in Figure 2, for the present investigation was of inside dimensions 305 mm $\times$ 305 mm. Entry and exit lengths of 1.5 m each were provided to optimize the velocity profile prior to the air entering the test section and to reduce flow fluctuations. Within the test section a heat exchanger 100 mm wide was mounted transverse to the air flow. This was constructed to represent a third-scale model of the Airedale EHA5 horizontal flow packaged air-conditioning unit fitted with a fin–tube heat exchanger. The

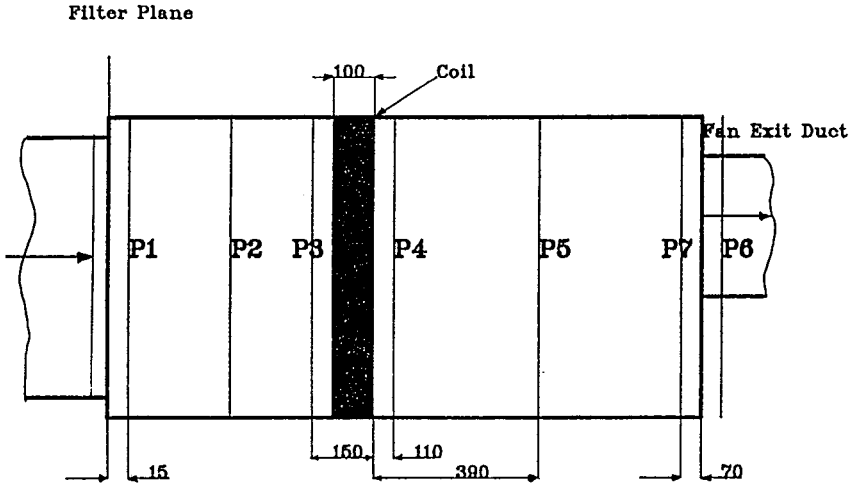

Figure 2. Position of test planes in EHA5 unit (all dimensions are in millimetres)

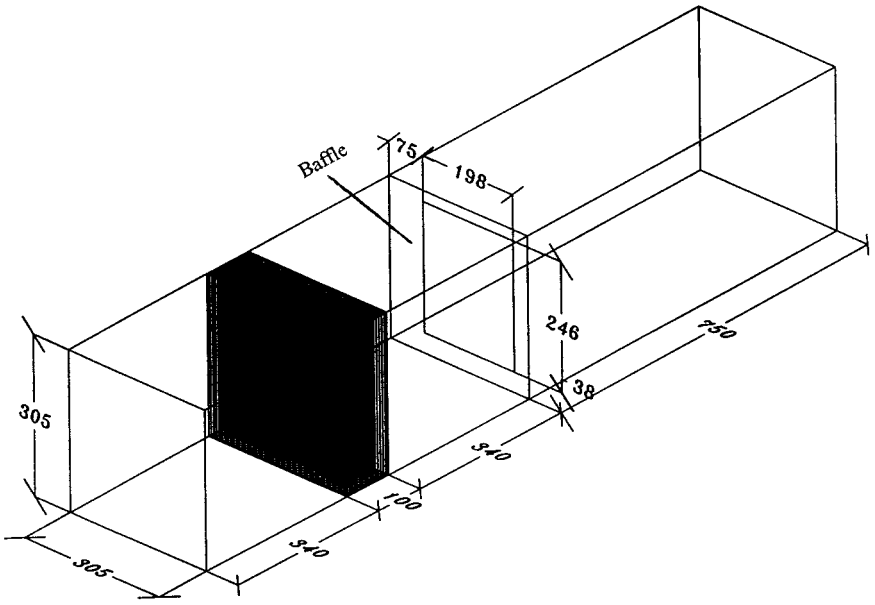

Figure 3. Geometry of simulated wind tunnel (all dimensions are in millimetres)

evaporator coil is a finned tube-type heat exchanger with five rows of small-diameter tubes arranged in staggered formation. The diameter of the tube is 10 mm and each row is stacked with 10 tubes. The baffle, which was installed to simulate the effects of the coil mounting frame in the Airedale EHA5 unit, thus introducing a source of turbulence and creating regions of recirculation downstream, was placed 340 mm downstream of the heat exchanger; the dimensions of the baffle aperture are given in Figure 3.

Using triple-hot-wire anemometry techniques, data were obtained at a transverse plane 10 mm downstream of the baffle, from which the orthogonal components of instantaneous velocity and hence Reynolds stresses could be obtained.

3. MODEL FORMULATION

It is assumed in the current investigation that the flow is steady and that the fluid can be treated as incompressible. Furthermore, no heat transfer is considered between air and its cooling medium, i.e. the flow is isothermal. Consequently, the conservation equations for such a flow are the well-known Reynolds-averaged Navier–Stokes equations and the mass continuity equations. In Cartesian tensor notation these can be expressed as

$$\frac{\partial U_j}{\partial x_j} = 0, \tag{1}$$

$$\rho U_j \frac{\partial U_j}{\partial x_j} = -\frac{\partial P}{\partial x_i} + \frac{\partial}{\partial x_j}\left[\mu\left(\frac{\partial U_i}{\partial x_j} + \frac{\partial U_j}{\partial x_i}\right)\right] - \frac{\partial}{\partial x_j}\rho\overline{u_i u_j}, \tag{2}$$

where the subscripts i and j can take values of 1, 2 and 3 and a repeated subscript indicates a summation. U_i and u_i denote the mean and instantaneous component of velocity in the orthogonal co-ordinate direction x_i respectively, p is the local pressure, ρ is the fluid density

and μ is the dynamic viscosity. The last term of the RHS, $\overline{u_i u_j}$, is collectively known as the Reynolds stresses. These arise from time averaging of the non-linear convection terms in the original momentum equations and have the appearance of stresses. They represent the effect of the turbulence on the mean flow field and their presence results in the number of unknowns exceeding the number of equations available, i.e. the system is not closed. The computation of turbulent flow is essentially a search for a model which can express the Reynolds stresses in terms of known or calculable mean flow quantities.

3.1. Turbulence model

A number of turbulence models have been developed over the years. Typical different-order models are the mixing length model, the two-equation k–ϵ model and Reynolds stress models. The two-equation k–ϵ model [3], which is of moderate complexity, has been extensively tested and proved to be adequate over a wide range of engineering applications. It can be regarded as a compromise between the simple but less accurate mixing length model and the accurate but more complex Reynolds stress models.

3.1.1. The k–ϵ model. The model employs the Boussinesq eddy viscosity hypothesis based on the analogy between molecular and turbulent motion. Hence

$$\rho\overline{u_i u_j} = \mu_t\left(\frac{\partial U_i}{\partial x_j} + \frac{\partial U_j}{\partial x_i}\right) - \frac{2}{3}\delta_{ij}k, \tag{3}$$

where μ_t is the eddy viscosity, k is the turbulence kinetic energy ($k = \frac{1}{2}\overline{u_i^2}$) and δ_{ij} is the Kronecker delta tensor, which is unity for $i = j$ and zero for $i \neq j$. The eddy viscosity hypothesis stems from the convenience associated with maintaining an approach for turbulent flows which is similar to that for laminar flows. In this model the eddy viscosity is related to the turbulence kinetic energy k and its dissipation rate ϵ as

$$\mu_t = \rho C_\mu k^2/\epsilon\,, \tag{4}$$

where k and ϵ are computed through their own transport–diffusion equations

$$\rho U_j \frac{\partial k}{\partial x_j} = \frac{\partial}{\partial x_j}\left(\frac{\mu_t}{\sigma_k}\frac{\partial k}{\partial x_j}\right) + P_k - \rho\epsilon, \tag{5}$$

$$\rho U_j \frac{\partial \epsilon}{\partial x_j} = \frac{\partial}{\partial x_j}\left(\frac{\mu_t}{\sigma_\epsilon}\frac{\partial \epsilon}{\partial x_j}\right) + C_{\epsilon 1}\frac{P_k \epsilon}{k} - C_{\epsilon 2}\frac{\rho\epsilon^2}{k}. \tag{6}$$

Here P_k is the production of turbulence kinetic energy,

$$P_k = \mu_t\left(\frac{\partial U_i}{\partial x_j} + \frac{\partial U_j}{\partial x_i}\right)\frac{\partial U_i}{\partial x_j}, \tag{7}$$

and C_μ, σ_k, σ_ϵ, $C_{\epsilon 1}$ and $C_{\epsilon 2}$ are turbulence model constants. The values adopted are $C_\mu = 0.09$, $\sigma_k = 1.0$, $\sigma_\epsilon = 1.3$, $C_{\epsilon 1} = 1.44$ and $C_{\epsilon 2} = 1.92$.

3.1.2. Reynolds stress models. Reynolds stress models can generally be divided into two classes: differential and algebraic. In the current work, only the Reynolds differential stress model was used. In this model, $\overline{u_i u_j}$ satisfies the transport equation

$$U_k \frac{\partial \overline{u_i u_j}}{\partial x_k} = P_{ij} + D_{ij} + \phi_{ij} - \epsilon_{ij}, \tag{8}$$

where the terms on the RHS are known as the shear stress production, diffusion, pressure strain and dissipation terms respectively. The shear stress production P_{ij} does not need to be modelled since it is simply the product of shear stress and strain rate, i.e.

$$P_{ij} = -\left(\overline{u_i u_k}\frac{\partial U_j}{\partial x_k} + \overline{u_j u_k}\frac{\partial U_i}{\partial x_k}\right), \tag{9}$$

whereas the other three terms must be modelled. For the diffusion term D_{ij} the gradient diffusion hypothesis [4] is used:

$$D_{ij} = -\frac{1}{\rho}\frac{\partial}{\partial x_k}\left(C_s \frac{k}{\epsilon}\overline{u_k u_l}\frac{\partial \overline{u_i u_j}}{\partial x_l}\right). \tag{10}$$

The modelling of the pressure strain terms ϕ_{ij} remains the most difficult task. It contains two types of process called slow and rapid parts:

$$\phi_{ij} = \overline{\frac{p'}{\rho}\left(\frac{\partial u_i}{\partial x_j} + \frac{\partial u_j}{\partial x_i}\right)} = \phi_{ij,1} + \phi_{ij,2}. \tag{11}$$

The former is modelled by Rotta's linear return-to-isotrophy approximation as

$$\phi_{ij,1} = -C_{1s}\frac{\epsilon}{k}\left(\overline{u_i u_j} - \frac{2}{3}k\delta_{ij}\right), \tag{12}$$

while the rapid part is usually represented by the 'isotropization of production' (IP) model of Launder *et al.* [5] as

$$\phi_{ij,2} = -C_{2s}\left(P_{ij} - \frac{2}{3}P_k\delta_{ij}\right), \tag{13}$$

It should be noted that there are extra wall reflection terms in the pressure strain correlation. However, owing to their complexity, these are not considered in the model. The stress dissipation ϵ_{ij} is modelled on the assumption that this process is locally isotropic and may thus be characterized by the dissipation of turbulence kinetic energy:

$$\epsilon_{ij} = \frac{2}{3}\delta_{ij}\epsilon, \tag{14}$$

where ϵ is from Equation (6).

C_s, C_{1s} and C_{2s} are the Reynolds stress model constants. The values adopted are $C_s = 0.22$, $C_{1s} = 1.8$ and $C_{2s} = 0.6$.

3.2. Heat exchanger model

The heat exchanger installed in the wind tunnel is of a finned tube type consisting of a large number of small-diameter tubes and very thin fins. The effect of the presence of these numerous solid objects in the flow field is twofold: (i) the volume available to the fluid is reduced compared with the nominal volume of the space considered; (ii) additional flow resistance is introduced. The complexity of the coil arrangement, and taking into consideration the nature of the geometry of the other components in the system, precludes modelling the flow through the heat exchanger in detail. A small control volume may contain a number of fins and tubes. Therefore it would be difficult to model the flow in such regions in detail, as a very fine grid would be required.

To circumvent this difficulty, a distributed resistance (porous medium) concept is adopted for the heat exchanger. The concept was initially developed by Patankar and Spalding [6] for simulating two-phase flows in a steam generator. Recently Shim *et al.* [7] used it to model the flow in the fuel assemblies of a reactor core. To describe the flow in a porous medium, the conservation equations are spatially averaged in a small control volume. For a detailed description of this spatial averaging process, see Reference [8]. The spatial averaging process introduces extra terms compared with the original unaveraged equations. For example, the Navier–Stokes equations with the k–ϵ model is a porous medium becomes

$$\frac{\partial K_{jk} U_k}{\partial x_j} = 0, \tag{15}$$

$$\rho \frac{\partial}{\partial x_j}(K_{jk} U_k U_i) = -\gamma \frac{\partial P}{\partial x_i} + \frac{\partial}{\partial x_j}\left((\mu + \mu_t) K_{jk} \frac{\partial U_i}{\partial x_k}\right) - \gamma R_{ij} U_j, \tag{16}$$

where γ is referred to as the volume porosity, defined as the ratio of the fluid volume to the nominal physical volume, K_{ij} is the area porosity and R_{ij} represents a distributed resistance (drag) to account for the combined effects of flow separation and turbulent diffusion in the small control volume. Both K_{ij} and R_{ij} are second-rank tensors in order to account for possible anisotropies in structure and resistance. The area porosity is defined as

$$A_i' = K_{ij} A_j, \tag{17}$$

where $A_i'$is the vector area available to fluid flow and A_i is an infinitesimal planar control surface of the vector area. In the current work, however, the area porosity was assumed to be isotropic. Hence $K_{jk} = \gamma$ for $j = k$ and $K_{jk} = 0$ for $j \neq k$. The volume porosity for the heat exchanger under study was calculated to be 0.85.

The resistance to the flow was calculated from appropriate empirical correlations which take into account the fin–tube geometry, fluid properties, local mass flow rate, etc. In practice the resistance is expressed in terms of a drag coefficient C_D defined as

$$C_D = \frac{2R}{\rho U^2}. \tag{18}$$

For a staggered tube configuration the following correlation [9] was used:

$$C_D = 0.618 + 0.491 \times 10^{-6} Re - 6.303 \times 10^{-12} Re^2 + 10.694 \times 10^{-18} Re^3 - 5.2 \times 10^{-24} Re^4, \tag{19}$$

where $Re = \rho U l / \mu$ is the Reynolds number and l is a length scale.

In a similar manner the form of Reynolds stress models in a porous medium can also be obtained [10].

4. BOUNDARY CONDITIONS

The governing equations described above constitute a system of coupled non-linear partial differential equations of elliptic nature. As such, boundary conditions must be prescribed on the whole surface of the physical domain. Three main types of boundary conditions are encountered in the calculation: inlet, outlet and wall.

At the inlet the values of velocity components are prescribed from experimental measurements. The turbulence kinetic energy and dissipation rate are difficult to obtain experimentally and thus are approximated from the relations

$$k_{\text{in}} = 0.003U_{\text{in}}^2, \qquad \epsilon = C_\mu k_{\text{in}}^{3/2}/l_{\text{in}}, \tag{20}$$

where l_{in} is a characteristic length scale that is approximated by the hydraulic diameter based on the inlet geometry. The turbulence intensity is typical for the conditions where the test was conducted.

At an outlet the pressure boundary is imposed. The velocities are determined in such a way that mass conservation should be satisfied.

On a wall the no-slip condition is applied. To avoid using an excessive number of grid points through the viscous sublayer, the well-known wall function method is employed. With this method the innermost region of the flow is omitted and an artificial boundary is applied inside the wall at a point some distance from the real wall. It is assumed that the near-wall region is in local energy equilibrium, so the profile of the non-dimensional velocity component parallel to the wall is logarithmic and the turbulence shear stress is constant. Thus

$$\frac{U}{\sqrt{(\tau_{\text{wall}}/\rho)}} = \frac{1}{\kappa} \ln\left(E_y \frac{\sqrt{(\tau_{\text{wall}}/\rho)}}{\nu} \right), \tag{21}$$

where τ_{wall} is the wall shear stress, E is a roughness parameter and κ is the von Karman constant. Once the velocity gradient and associated wall shear stress have been evaluated, the near-wall values of turbulence kinetic energy and dissipation rate can be calculated as

$$k = |\tau_{\text{wall}}|/\sqrt{(\rho C_\mu)}, \qquad \epsilon = C_\mu^{3/4} k^{3/2}/\kappa y. \tag{22}$$

The values of Reynolds stresses at the wall are calculated by linear extrapolation from values in the control volume interior to the flow. This ensures that the effect of the wall on the flow is calculated correctly.

5. NUMERICAL PROCEDURE

The partial differential equations are solved numerically on a non-staggered grid using a conservative finite volume method (FVM). With non-staggered grids the physical domain is subdivided into a number of finite cuboidal control volumes and all variables are collocated at the centroids of the hexahedrons, as shown in Figure 4. Finite difference equations are obtained by integrating the differential equations over each control volume and then treating each term by an appropriate differencing scheme. The advection terms in the equations are treated by a hybrid scheme, while a central differencing scheme is used for the other terms. The resulting algebraic equation for the variable ϕ at node P can be cast into the general form

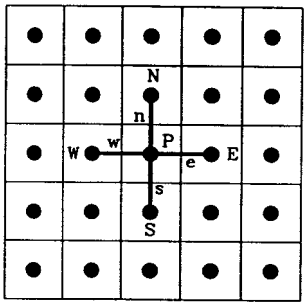

Figure 4. Nodal arrangement

$$A_P\phi_P = \sum_{nb} A_{nb}\phi_{nb} + S_{\phi,u}, \tag{23}$$

where the As are the matrix coefficients representing the combined influence of convection and diffusion on the corresponding faces of the control volume and $A_P = \Sigma_{nb} A_{nb} + S_{\phi,p}$. Σ_{nb} denotes the summation over the nearest-neighbouring nodes (nb = U, D, W, E, S, N). The source term should be linearized in such a way as to ensure that the matrix coefficients are positive and diagonally dominant.

The coupled set of algebraic equations is solved iteratively using a line-by-line alternating direction method based on the tridiagonal matrix algorithm (TDMA). The momentum equations are first solved with a guessed pressure field. Corrections to the guessed velocity fields and pressure field are made to satisfy the continuity equation according to the SIMPLEC algorithm [11]. Then the velocities and pressure are updated and the turbulence model equations are solved. The solution is assumed converged when the sum of the normalized mass residuals in the entire computational domain is less than a prescribed tolerance value. To ensure convergence, the variables are often underrelaxed in the iteration. The commonly used iterative algorithms are Gauss–Seidel and SOR. They have a simple structure and are cheap to use, if the iterations converge. However, for many practical problems, convergence can be slow, with small relaxation factors, or non-existent. To accelerate convergence, it may be necessary to use a more efficient full field solver such as Stone's strongly implicit procedure (SIP) or preconditioned conjugate gradient (ICCG) algorithms.

The computation of convective coefficients in Equation (17) requires a knowledge of the velocity components at the control volume faces. With the use of a non-staggered grid system, however, the velocities are not stored at the faces but must be interpolated from those at the control volume centres. The naive prescription for this would be to use a weighted linear interpolation, which can lead to 'checkerboard'-type oscillations. These are dealt with by the Rhie–Chow momentum interpolation algorithm [12]. Here the coefficients are linearly interpolated, but the pressures at the neighbouring cell node are used rather than averaging the pressure gradients for the control volumes. In this way, strong velocity–pressure coupling is enforced.

The principle of the main method of solution, described above, has been implemented in a commercial computational fluid dynamics code CFDS-FLOW3D (release 2.4 [13]) developed by the United Kingdom Atomic Energy Authority (Harwell). It is a general-purpose programme for the prediction of laminar and turbulent flows with heat and mass transfer in three-dimensional geometries. The computation was performed on a Convex Supercomputer at the University of London Computer Centre (ULCC).

6. RESULTS AND DISCUSSION

For the geometry shown in Figure 3 a rectilinear grid system is employed. The grid has 37 cells in the axial (x), 31 in the lateral (z) and 21 in the vertical (y) direction. Increasing the number of grid points and the grid density location by a factor of two in each co-ordinate direction, up to the maximum achievable with the current computer system, yielded a numerical solution that is virtually identical to that obtained using the original $37 \times 31 \times 21$ grid. Figure 5 is a three-dimensional view of the grid system used in the calculation. Figures 6 and 7 show the grid distribution in a representative xy- and yz-plane respectively. It can be seen that a non-uniform grid distribution is adopted. The cells are concentrated in the baffle region so that the grid resolution is fine enough to resolve the secondary flow there. Furthermore, the grid used for the simulation was non-symmetrical because of the baffle geometry.

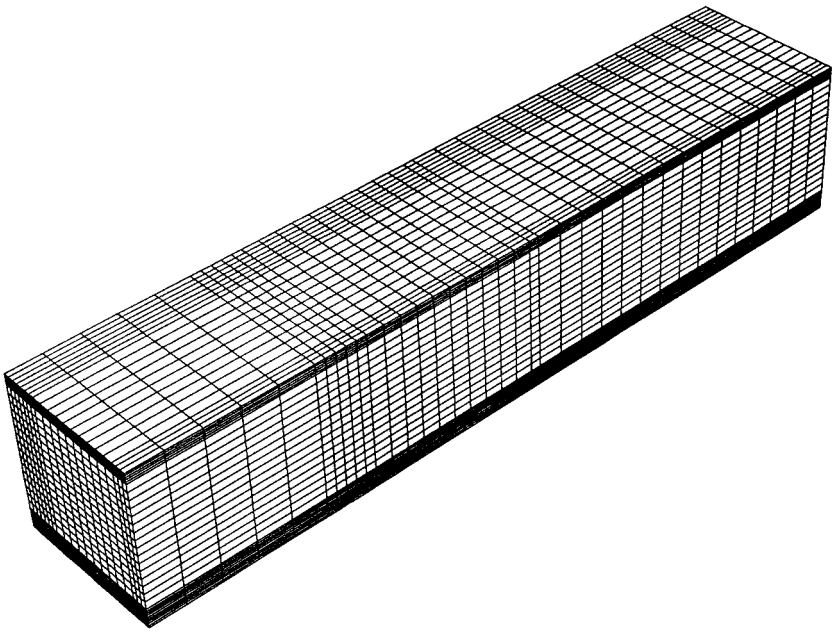

Figure 5. Computational grid ($37 \times 31 \times 21$)

The fluid was observed to enter the wind tunnel with a nearly uniform axial velocity profile of 2.6 m s^{-1} and was discharged to the atmosphere at the exit. The barometric pressure at the exit was 1.013 bar. In the calculation the density and kinematic viscosity of the air were taken at a room temperature of 22°C to be 1.2 kg m^{-3} and 1.465×10^{-5} m^2 s^{-1} respectively. Based on the inlet flow condition and geometry, the Reynolds number for the flow was calculated to be 5.84×10^4.

The air flow patterns in the wind tunnel, predicted using the k–ϵ model, are shown for six planes in Figures 8–10. It can be seen that the flow is mainly in the axial direction upstream of the baffle. As the flow approaches the baffle, it starts to converge. Downstream of the baffle a region of recirculation is formed and there is a strong secondary flow (Figure 9). The effect of the wider baffle dimension in the horizontal plane on the size of the recirculation is clearly illustrated with reference to Figures 8 and 9.

The comparisons between the measured and predicted velocity profiles are displayed in Figure 11 for the k–ϵ model and in Figure 12 for the Reynolds differential stress model. It is

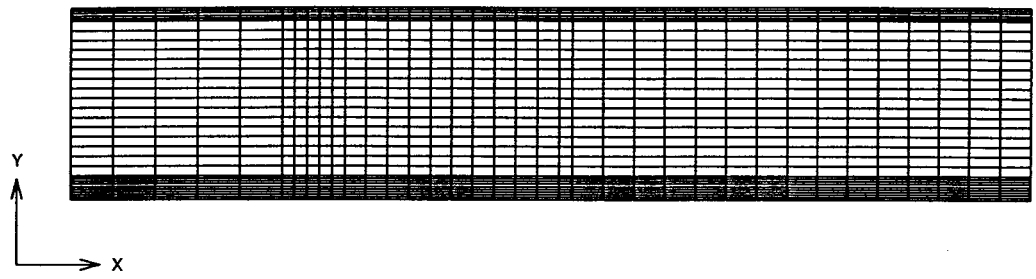

Figure 6. Grid distribution in an xy-plane

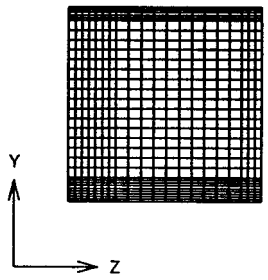

Figure 7. Grid distribution in a yz-plane

interesting to note that the curves for the predicted axial velocity (U-velocity) for both turbulence models show good agreement with the experimental data in the centre of the duct, including the edge of the recirculation zones created by the upper and lower baffles. However, in the regions $y < 70$ and $y > 250$ the predicted axial velocity (U-velocity) deviates considerably from the measurements. This may be due to some shortcomings of the mathematical model itself or to problems associated with the use of the hot-wire anemometer probe in strong recirculating flow. It is worth pointing out that the standard k–ϵ model is only valid for high-Reynolds-number turbulent flows. Its use for low-Reynolds-number turbulent flows may lead to errors. Another contributing factor may be the limited accuracy of the wall function method in the boundary layer region, as well as the matching ability of the higher-order discretization procedure in this area. It may be more appropriate and accurate to employ a low-Re version of the k–ϵ model [14] instead. However, this model needs a much more refined grid along the solid boundaries and was beyond the capabilities of the computer system used.

The comparisons in the case of the V- and W-velocity components appear to exhibit similar characteristics, although in these cases the result is less pronounced owing to the low levels of velocity. A careful inspection of Figures 11 and 12 reveals that on the whole the predictions

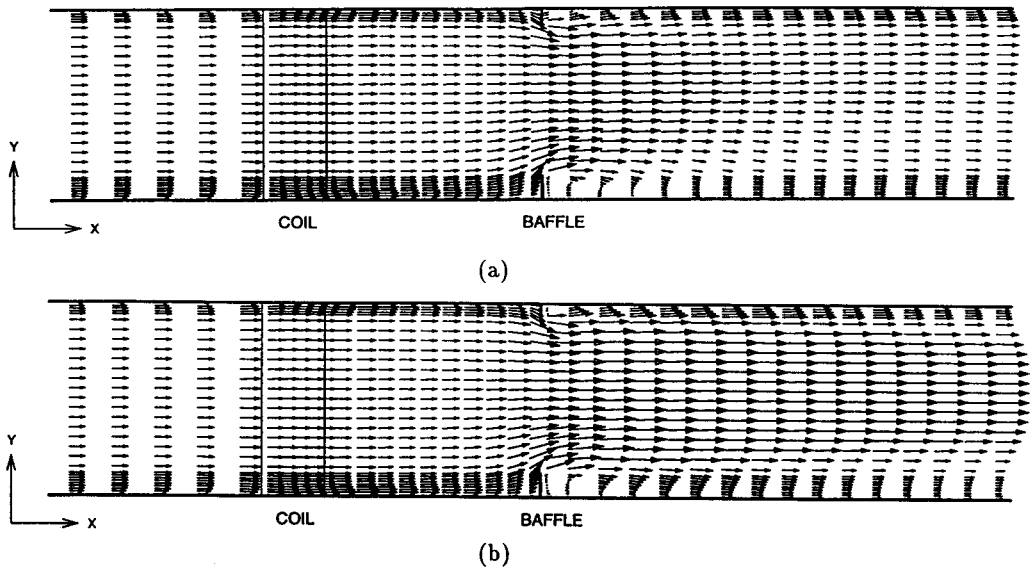

Figure 8. Predicted velocity profile on a vertical plane (k–ϵ model): (a) plane $z = 125$ mm; (b) plane $z = 225$ mm

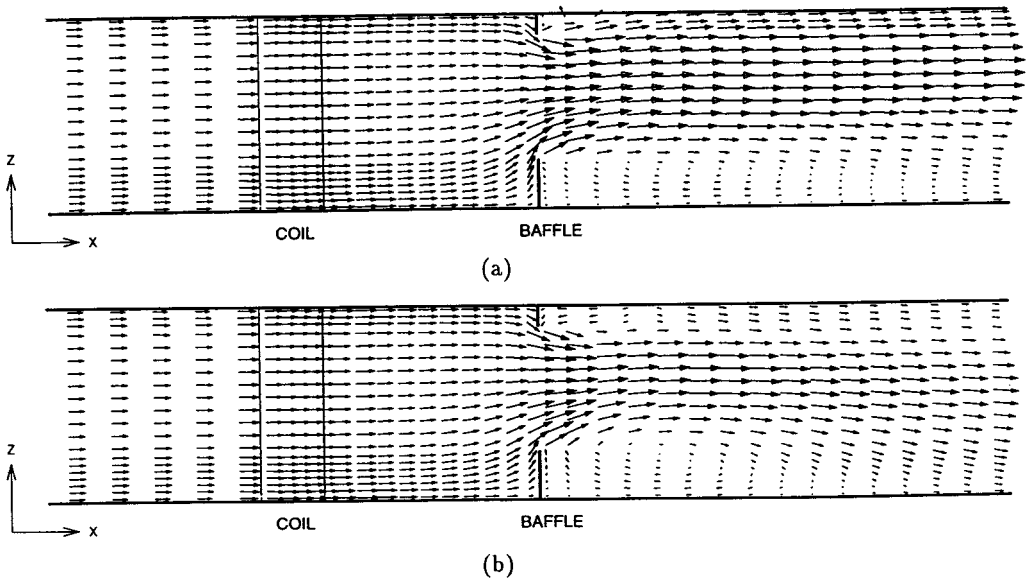

Figure 9. Predicted velocity profile on a horizontal plane (k–ϵ model): (a) plane $y = 200$ mm; (b) plane $y = 280$ mm

from the k–ϵ model and the Reynolds stress model are very close, with the former producing a slightly better fit to the experimental profiles. Consequently, the use of the k–ϵ model for predicting the turbulent recirculating flows in air-conditioning units appears to be the most suitable.

The predicted and measured Reynolds shear stresses are compared in Figure 13. The measured profiles indicate that all three shear stress components are nearly zero across the measured plane. As a result, the turbulence here can be regarded as isotropic. This further supports the case for the use of the k–ϵ model. In terms of $\overline{uv}$ and $\overline{vw}$ the numerical results agree well with the measurements. However, there is some discrepancy between the two with regard to $\overline{uw}$. The stress model has overestimated its values by roughly 1.0 $m^2\ s^{-2}$ across the whole area. It appears that further investigations may be needed to improve the accuracy of the Reynolds stress model. One measure to be taken is the inclusion of wall reflection terms in the pressure strain terms of the model.

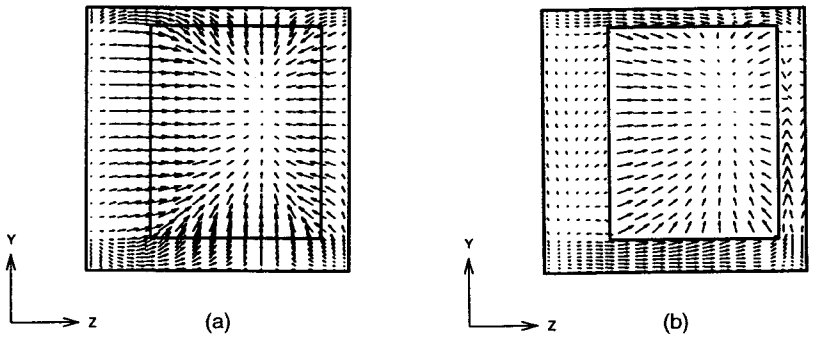

Figure 10. Predicted secondary flow pattern (k–ϵ model): (a) 20 mm upstream of baffle; (b) 10 mm downstream of baffle

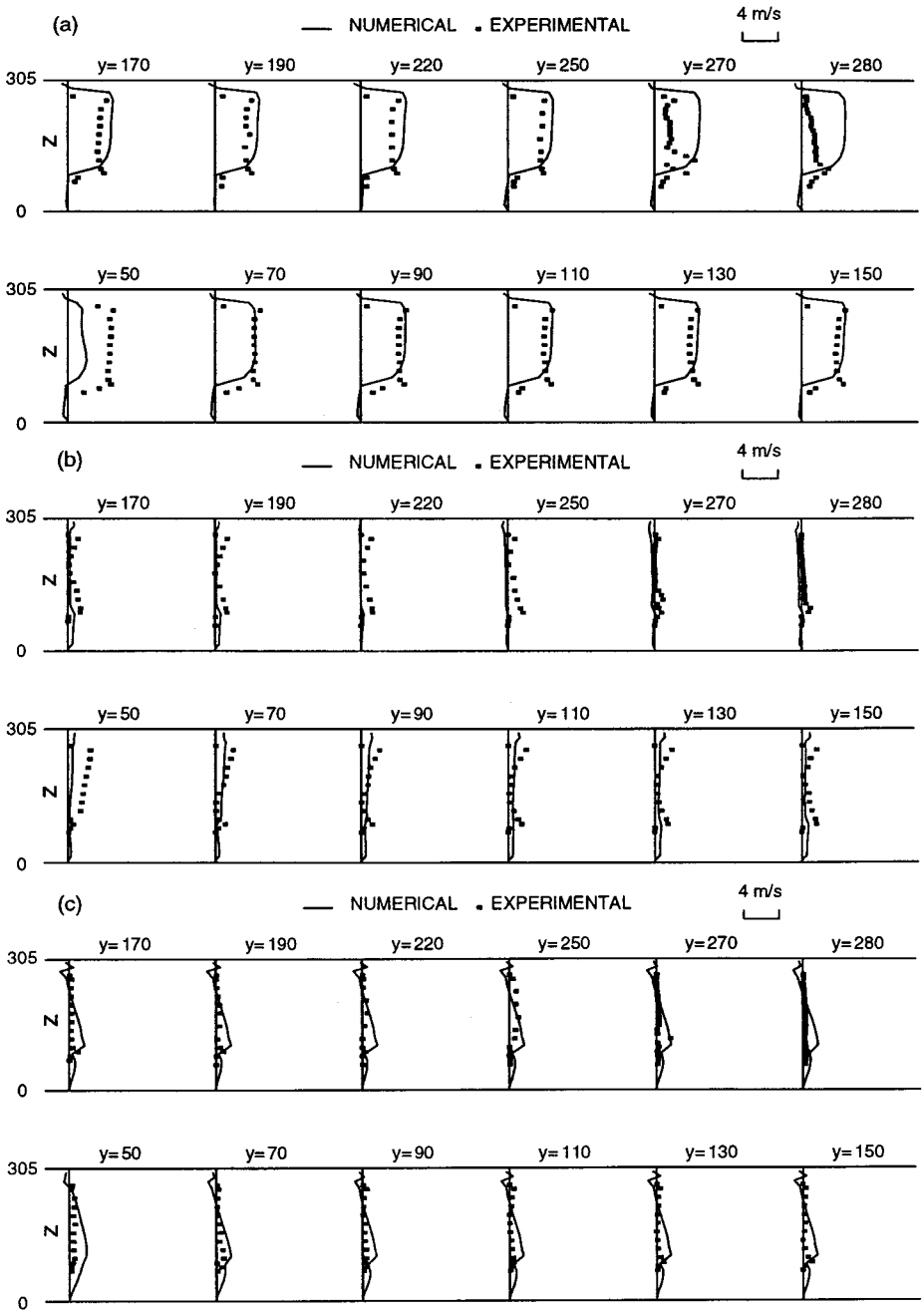

Figure 11. Predicted and experimental velocity profiles 10 mm downstream of baffle (k–ϵ model): (a) U-velocity; (b) V-velocity; (c) W-velocity

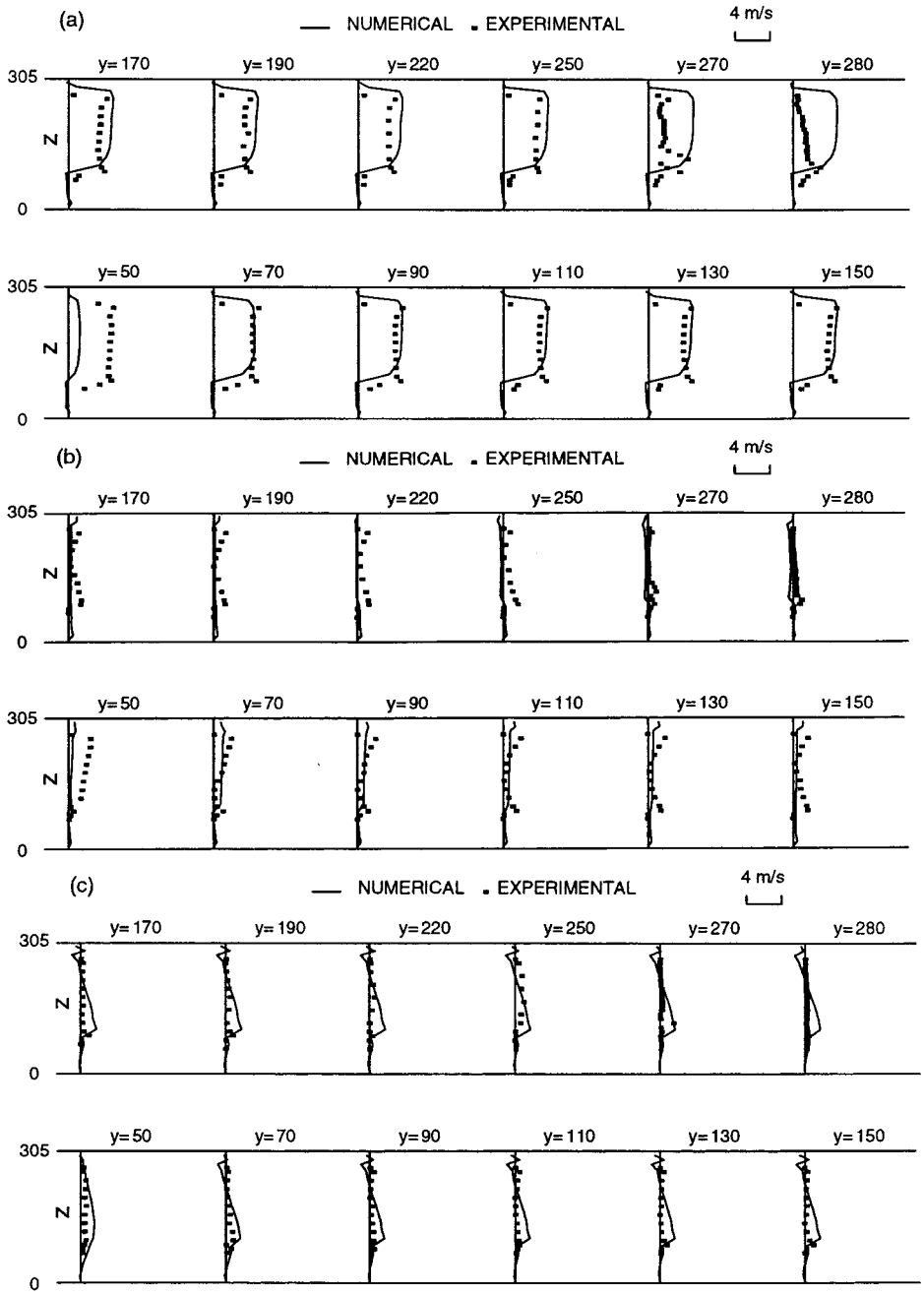

Figure 12. Predicted and experimental profiles 10 mm downstream of baffle (Reynolds stress model): (a) U-velocity; (b) V-velocity; (c) W-velocity

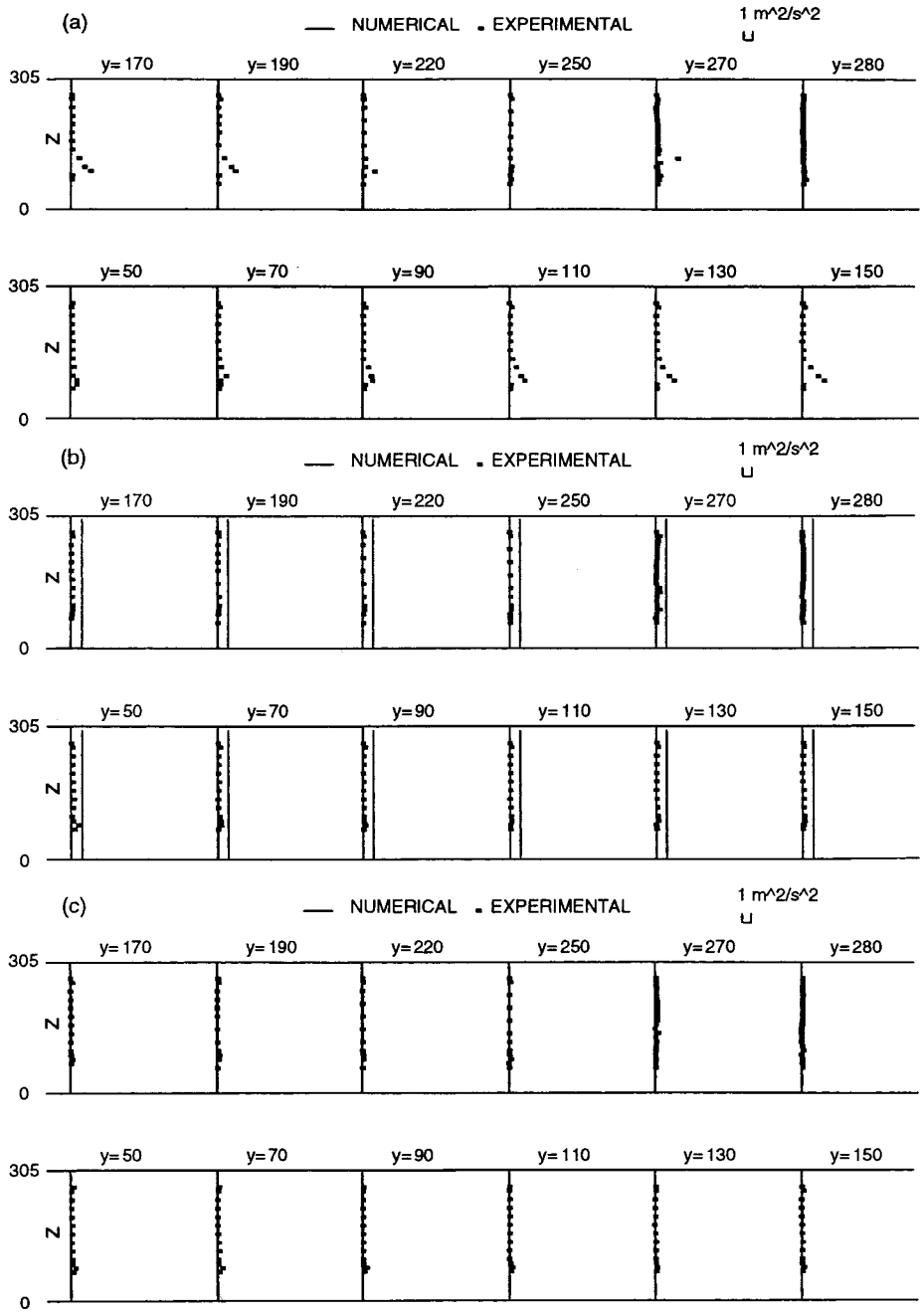

Figure 13. Predicted and experimental Reynolds shear stresses 10 mm downstream of baffle: (a) $\overline{uv}$; (b) $\overline{uw}$; (c) $\overline{vw}$

7. CONCLUSIONS

The investigation, carried out with the purpose of providing supplementary validation data, has provided further evidence that CFD techniques can be employed to obtain good predictions of a turbulent air flow pattern that includes regions of recirculation. It was found that the predicted air velocities in the three directions were in good agreement with those measured using a three-wire anemometer probe except in regions where flow recirculation occurred, with the k–ϵ model performing marginally better than the Reynolds stress model.

ACKNOWLEDGEMENTS

The work described here was conducted under a joint sponsorship by the Engineering and Physical Science Research Council (EPSRC) and Department of Trade and Industry (DTI) of the United Kingdom. The authors would also like to thank Airedale International Air Conditioning Ltd. (Leeds) for their assistance in obtaining the experimental data and CFDS (UKAEA) for the use of their CFDS-FLOW3D code.

APPENDIX A. NOMENCLATURE

A	convection–diffusion coefficient
C_s, C_{1s}, C_{2s}	Reynolds stress model constants
C_μ, $C_{\epsilon 1}$, $C_{\epsilon 2}$	k–ϵ model constants
D_{ij}	diffusion of Reynolds stresses
E	roughness length
k	turbulence kinetic energy
K_{ij}	area porosity tensor
P	static pressure
Pe	Peclet number
P_{ij}	production of Reynolds stresses
P_k	product of turbulence kinetic energy
r	volume porosity
R_{ij}	distributed resistance tensor
S	source/sink term
u	fluctuating velocity in axial direction
u_i	fluctuating velocity
$\overline{u_i u_j}$	Reynolds stresses
U	time-averaged mean velocity in axial direction
U_i	time-averaged mean velocity
v	fluctuating velocity in lateral direction
V	time-averaged mean velocity in lateral direction
w	fluctuating velocity in vertical direction
W	time-averaged mean velocity in vertical direction
x, y, z	co-ordinates in axial, lateral and vertical direction
x_i	co-ordinate in ith direction

Greek letters

Γ	diffusion coefficient

δ_{ij}	Kronecker delta
ϵ	dissipation rate of turbulence kinetic energy
ϵ_{ij}	dissipation of Reynolds stresses
μ	dynamic viscosity
ν	kinematic viscosity
ρ	fluid density
σ_k, σ_ϵ	turbulent Prandtl numbers
ϕ	general variable

REFERENCES

1. Z.G. Xu, D.H.T. Gotham and M.W. Collins, 'Numerical modelling of turbulent flow through packaged and simulated air-conditioning units', *Thermo-Fluids Engineering Research Centre*, *RM188*, City University, London, 1993.
2. J.E.R. Coney, H. Kazeminejad and C.G.W. Sheppard, 'Dehumidification of turbulent air flow over a thick fin; an experimental study', *Proc. Inst. Mech. Engng.*, **203**, (1989).
3. W.P. Jones and B.E. Launder, 'The prediction of laminarization with a two-equation model of turbulence', *Int. J. Heat Mass Transfer*, **15**, 301–314 (1972).
4. B.J. Daly and F.H. Harlow, 'Transport equations of turbulence', *Phys. Fluids*, **13**, (1970).
5. B.E. Launder, G.J. Reece and W. Rodi, 'Progress in development of a Reynolds-stress turbulence closure', *J. Fluid Mech.*, **68**, 537–566 (1975).
6. S.V. Patankar and D.B. Spalding., 'Computer analysis of the three dimensional flow and heat transfer in a steam generator', *Forsch. Ing-Wes.*, **44**, (1978).
7. S.Y. Shim, P.T. Wan, D.K. Baxter and R.L. Hembroff, 'A study of confined turbulent jets under suction and counter current flows', in *Numerical Methods in Laminar and Turbulent Flow*, Pineridge, Swansea, 1989.
8. J.H. Cushman, *Dynamics of Fluids in Hierachical Porous Media*, Academic, New York, 1990.
9. G.F. Hewitt, *Handbook of Heat Exchanger Design*, Hemisphere, New York, 1990.
10. J.D. Wilson, 'A second-order closure model for flow through vegetation', *Boundary-Layer Meteorol.*, **42**, 371–392 (1988).
11. J.P. Van Doormal and C.D. Raithby, 'Enhancements of the SIMPLE method for predicting incompressible fluid flows', *Numer. Heat Transfer*, **7**, (1984).
12. C.M. Rhie and W.L. Chow, 'A numerical study of the turbulent flow past an isolated airfoil with trailing edge separation', *AIAA J.*, **21**, 1525–1532 (1993).
13. A.D. Burn, I.P. Jones, J.R. Kightley and N.S. Wilkes, 'Harwell-FLOW3D, release 2.4: user manual', *Harwell Rep. AERE-R*, 1990.
14. B.E. Launder and B.T. Sharma, 'Application of the energy dissipation model of turbulence to the calculation of flow near a spinning disc', *Lett. Heat Mass Transfer*, **1**, 131–138 (1974).